New Sulfonated Aramide Nanoparticles and Their Copper Complexes with Anomalous Dielectric Behavior

Hammed H. A. M. Hassan,[1] Amel F. Elhusseiny,[1] Amr M. Sweyllam,[2] Robert J. Linhardt[3]

[1]Chemistry Department, Faculty of Science, Alexandria University, P. O. Box 2, Moharram Beck, Alexandria 21568, Egypt

[2]Physics Department, Faculty of Science, Alexandria University, Moharrem Bee, Alexandria, Egypt

[3]Department of Chemistry and Chemical Biology, Center for Biotechnology and Interdisciplinary Studies, Rensselaer Polytechnic Institute, Biotech Center 4005, 110 8th Street, Troy, New York 12180-3590

Correspondence to: H. H. A. M. Hassan (E-mail: hassan10@safwait.com)

ABSTRACT: We report the preparation of thermally stable spherical sulfonated aramides nanoparticles and their copper(II) complexes. Metal chelation with copper ions furnished polymeric complexes in a 1 : 2 ratio with square planar geometries as judged by their IR, UV, electron spin resonance, and elemental analysis data. The direct-current electrical conductivities demonstrated the semiconducting nature of the polymeric particles and their copper complexes. Dielectric loss analysis studies showed spectral peaks appearing at characteristic frequencies, which suggested the presence of relaxing dipoles in all of the polymers. All loss peaks were shown on a linear frequency scale and appeared in the range of 1 decade, and no overlap was observed in any of the samples, whereas in the normal polymer's dielectric loss behavior, each peak covered more than 1 decade. Moreover, the peak positions did not change with increasing temperature; this indicated a nonactivated process. The reported dielectric results revealed anomalous behavior, which has not been reported before for such polymeric analogues, as the polarization in these cases was limited by nonthermal forces, and a steady-state constant polarization was produced by an applied field. A simple method for the formation of a microporous semiconducting thin film of a polymer derived from isophthalic acid and diaminodiphenylsulfone is described. © 2012 Wiley Periodicals, Inc. J. Appl. Polym. Sci. 128: 310–321, 2013

INTRODUCTION

Aromatic polyamides are high-performance materials because of their superior thermal and mechanical properties; this makes them useful for advanced technologies. These polymers are finding increasing demand as advantageous replacements for metals and ceramics in currently used products and even as new materials in novel technological applications.[1–4] However, the extremely high transition temperatures of commercial aramids and their poor solubility in common organic solvents give rise to processing difficulties and limit their applications. As a result, recent basic and applied research has focused on enhancing their processability and solubility to broaden the scope of their technological applications.[5–12] The incorporation of flexible bonds onto the polymer backbone often increases its solubility by altering the crystallinity and intermolecular interactions.[13–15] In particular, an improvement in the solubility without extreme loss of the thermal stability can be obtained by the introduction of sulfonyl groups that are more active than ether or ketone groups in disrupting chain stiffness.[16–19]

Currently, tremendous effort has been devoted to opening up various facile methodologies for the production of nanostructured materials with novel morphologies. Because materials with fascinating new architectures can exhibit unique physicochemical properties, the nanomaterials produced in this study are of considerable interest as potential components for chemical/biochemical sensors, optoelectronic and nanoelectronic devices, and applications in nanobiotechnology.[20] Among various nanostructured materials, those with well-defined discrete architectures, typically exemplified by nanofibers, nanotubes, nanorods, nanospheres, nanocubes, and others, have so far been intensively investigated because of their extraordinary physicochemical properties. Many such inorganic-based systems have been developed,[21] whereas examples of organic-based systems are less numerous.[20(a,d,e,f)] In contrast to inorganic nanomaterials, organic nanostructures have peculiar electronic and optical properties and can afford impressive variety, flexibility in molecular design, and tunability of physicochemical properties.[20] This

makes organic-based nanostructures promising candidates for nanoscience and nanotechnology. Consequently, an exploration of the fabrication of organic nanostructures with unique and well-defined morphologies represents an important issue for intense exploration.

Semiconductor nanomaterials have attracted significant attention in research and for applications in a variety of areas, including energy conversion, sensing, electronics, photonics, and biomedicine. Parameters such as size, shape, and surface characteristics can be varied to control their properties for different applications of interest.[22–25] For many applications, it is highly desirable to have greater flexibility in controlling and altering the properties and functionalities of materials. One approach is to use hybrid nanomaterials that have properties different from those of single component nanomaterials. The use of multiple components offers a higher degree of flexibility for altering and controlling the properties and functionalities of nanomaterials. *Hybrid nanomaterials* can be generally defined as nanomaterials that contain more than one component. Examples include doped nanomaterials and composite nanomaterials.[26] The interest in using the unique properties of hybrid nanostructures for practical applications has increased with deeper understanding and an ability to tailor these materials. A huge variety of materials have already been synthesized and incorporated in devices, demonstrating their potential to enhance the performance of currently used technology.[27] The transition from fundamental science to industrial application requires an even deeper understanding and control of morphology and composition at the nanoscale. The size reduction of well-known materials into the nanometer regime and the realization that novel nanostructures can improve device performance has led to many discoveries. For instance, the size-dependent physical properties observed in one-dimensional nanomaterials[28] have included photon absorption and emission, such as in nanoscale avalanche photodiodes, metal-to-insulator transition in a material, and quantized or ballistic transport characteristics. The opportunity to investigate and evaluate novel physical properties in one-dimensional materials, the controlled fabrication of high-quality nanowires, and their growth mechanisms has attracted tremendous attention. Thus, the integration of high-aspect-ratio nanostructures into devices requires additional efforts in both engineering and materials science to control these processes on the atomic scale.

As a part of an ongoing research project directed toward the construction of new types of semiconducting aramide nanoparticles,[29–31] we report the synthesis and characterization of sulfonated aramides containing pyridine on the nanoscale by precipitation polymerization.[32] Previous researchers have focused on the systematic study of the synthesis and thermal stability of some aromatic thermoplastics containing sulfone groups.[33] The incorporation of copper into these polymers has also been studied with the aim of obtaining thermally stable nanosized semiconducting polyamide–copper(II) complexes. It is interesting to correlate the structure–property relationships, in particular, the influence of the pyridine nitrogen atom position on the polymer properties. For example, the *n* electrons of the pyridine N atom can be involved in linear conjugation; this can potentially impact the electrical properties of the resulting polymer.[34]
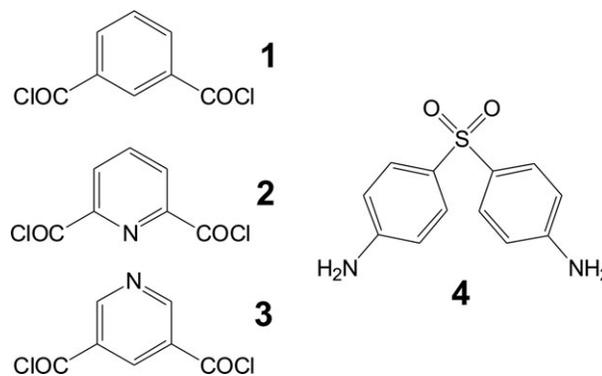

Figure 1. Monomers used in the polycondensation process.

EXPERIMENTAL

Materials

Isophthaloyl dichloride (**1**), pyridine-2,6-dicarbonyl dichloride (**2**), and pyridine-3,5-dicarbonyl dichloride (**3**; Figure 1) were made from commercial isophthalic acid (Merck, Darmstadt, Germany), pyridine-2,6-dicarboxylic acid (Aldrich, Taufkirchen, Germany), and pyridine-3,5-dicarboxylic acid (Aldrich, Taufkirchen, Germany), respectively, according to literature procedures.[35,36] Commercial 4,4′-diaminodiphenylsulfone (**4**), hydrated cupric acetate, and the solvents 1,4-dioxane (Aldrich, Taufkirchen, Germany) and dimethyl sulfoxide (DMSO; Aldrich, Taufkirchen, Germany) were used as purchased without purification.

Measurements

IR spectra (KBr pellets, 3 mm thick) were recorded on a PerkinElmer IR spectrophotometer (FTIR 1650, Santa Clara, CA) within the wave-number range $\upsilon = 600–4000$ cm^{-1} at 25°C.

Absorbance spectra were measured with a UV 500 UV–visible spectrometer (Thermo Electron Scientific; Madison, WI) at room temperature in DMSO with a polymer concentration of 2 mg/10 mL.

Differential thermogravimetric (DTG) analyses were carried out in the temperature range from 20 to 400°C in a stream of nitrogen on a Shimadzu DTG 60H thermal analyzer (Columbia, MD). These analyses were carried out in a platinum crucible under a nitrogen atmosphere with a 30 mL/min flow rate and a heating rate 10°C/min. Differential scanning calorimetry (DSC)–thermogravimetric analysis was carried out with SDT-Q600-V20.5-Build-15 (TA instruments; Eschborn, Germany).

Electron spin resonance (ESR) measurements of powder samples were recorded at room temperature with X-band microwave frequency as the first derivative on a Bruker spectrometer (Madison, WI) with 100-kHz magnetic field modulation with diphenyl picryl hydrazyl as a reference material.

Dielectric measurements were carried out in the frequency range from 0.1 to 5000 kHz with a Hioki 3532 inductance capacitance resistance tester (LCR) (Hioki Corporation, Japan) at different temperatures ranging from room temperature up to about 90°C.

Electrical measurements were carried in a vacuum chamber (10^{-2} Torr), and at the beginning of the measurements, the sample was heated to 50°C for about 15 min *in vacuo* to

eliminate humidity. The polymer powder was pressed to form discs 10 mm in diameter and 1mm thick. Silver electrodes were deposited on both sides of the sample surface by thermal evaporation, and two copper wires were fixed on the sample with conducting silver paint.

Inherent viscosities (η_{inh}'s) were measured at a concentration of 0.5 g/dL in DMSO at 30°C with an Cannon-Ubbelohde viscometer; Giza Egypt. Elemental analyses were performed at the Microanalytical Unit, Cairo University.

Copper contents were estimated complexometrically by ethylene diamine tetraacetic acid and pyridyl azonaphthol as an indicator.[37] Briefly, analysis of the copper followed decomposition of their complexes with a mixture of concentrated nitric and hydrochloric acids (1 : 1 v/v). The resultant residues were diluted by distilled water (100 mL), neutralized with NaOH (until the formation of blue color), acidified with acetic acid to pH 5, and then titrated with ethylene diamine tetraacetic acid.

The morphologies of the polymer nanoparticles were observed by scanning electron microscopy (SEM; JEOL-JSM5300 JEOL; Tokyo, Japan). The samples were sonicated in deionized water for 5 min and deposited onto carbon-coated copper mesh, air-dried, and sputter-coated with gold before examination.

Polymer Particle Synthesis (Poly [N-(4-((4-aminophenyl)sulfonyl)phenyl)-3-formylbenzamide 5, poly [N-(4-((4-aminophenyl)sulfonyl)phenyl)-6-formylpicolinamide] 6, poly [N-(4-((4-aminophenyl)sulfonyl)phenyl)-5-formylnicotinamide] 7; General Method)

The diacid chlorides (**1–3**; 0.5 mmol) and the diamine 4,4'-diaminodiphenylsulfone (**4**; 0.5 mmol) were each dissolved in 50 mL of dioxane. Distilled water (5 or 15 mL) was added to the solution of the diamine followed by addition of the entire acid chloride solution at once. The resulting turbid solution was ultrasonicated at 42 KHz in a water bath (25°C) for a period of 30 min. The polymer colloidal solution was extracted by centrifugal separation for 15 min at 15,000 rpm, and the resulting precipitate ($\sim$ 40% yields) was carefully washed with methanol and water to purify the product of any unreacted monomer. The polymer samples were then dried at 100°C for 10 h and then kept in a vacuum desiccator.

Preparation of the Cu(II) Complexes Cu 5–Cu 7 (General Method)

To a stirred solution of 0.10 mol of polyamide (**5–7**) in 25 mL of DMSO, Cu(OAc)$_2$·H$_2$O (0.12 mol) was added portionwise. The mixture was vigorously stirred at 90°C for 10 h and then poured while hot onto a large amount of crushed ice and water. The dark-colored precipitate was filtered, washed carefully with hot methanol and water, dried at 100°C for 10 h, and then kept in a vacuum desiccator.

RESULTS AND DISCUSSION

Synthesis of the Aramide Nanoparticles

The use of inherently nanostructured conjugated aramides as components for nanoelectronics is a promising route to future high-density nanochips.[38] Conjugated polymers can be synthesized in a precisely controlled way to form many different nano-
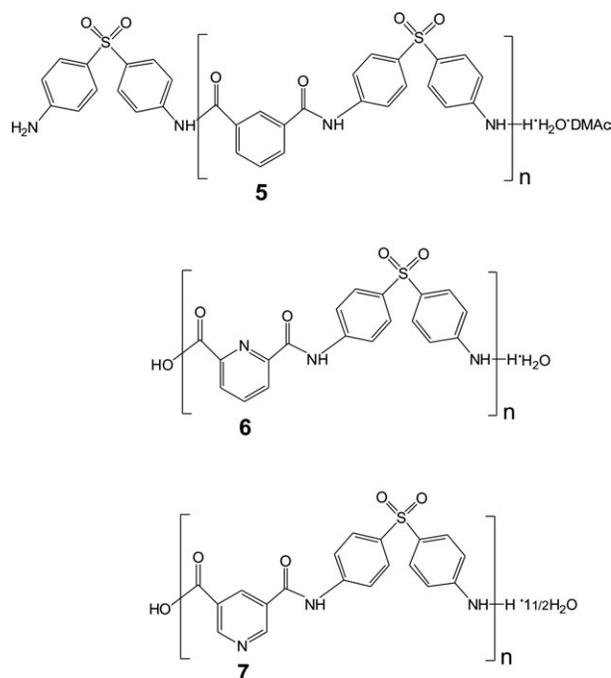
Figure 2. Chemical structures of aramides 5–7.

scale structures down to the molecular scale. Polymeric aromatic nanoparticles can be prepared by either emulsion or interfacial polymerization. Additionally, a popular method used for polymeric nanoparticle preparation is solvent displacement, also referred to as *nanoprecipitation*.[32] This method involves the dissolution of the monomers in an organic, water-miscible solvent, which is then added to the aqueous phase in the presence or absence of a surfactant. Upon addition to the aqueous phase, the organic solvent immediately diffuses out; this leads to the formation of nanoparticles. The aromatic acid chlorides (Figure 1), namely, **1, 2,** and **3**, used in this investigation were prepared by reactions of their corresponding dicarboxylic acids with thionyl chloride in the presence of few drops of dimethylformamide.[35,36] The polyamide nanoparticles **5–7** (Figure 2) were prepared by the ultrasonication of 0.5 mmol of the diamine (**4**) with 0.5 mmol of the acid chlorides (**1–3**) in a total of 105 mL of dioxane solution containing distilled water (5 mL; i.e., 50/5 mL v/v of a dioxane–water diamine solution and 50 mL of dioxane acid chloride solution) followed by centrifugal separation. SEM photographs of the products sulfonated aramide nanoparticles prepared in 1,4-dioxane/water (100/5). under these conditions are shown in Figure 3. The average diameters of the particles were estimated from SEM images and selected at random. The average diameter of the particles ranged from 200 to 300 nm, and the interconnection between particles was present to a greater or lesser extent. Interestingly, the average diameter of these particles decreased as the water content increased. Thus, ultrasonication of 0.5 mmol of the diamine (**4**) with 0.5 mmol of the acid chlorides (**1–3**) in a total of 115 mL of dioxane solution containing distilled water (15 mL; i.e., 50/15 mL v/v of a dioxane–water diamine solution and 50 mL of dioxane acid chloride solution) furnished the polymeric nanoparticles **5$_b$–7$_b$**. The average diameters were 106, 107, and 230
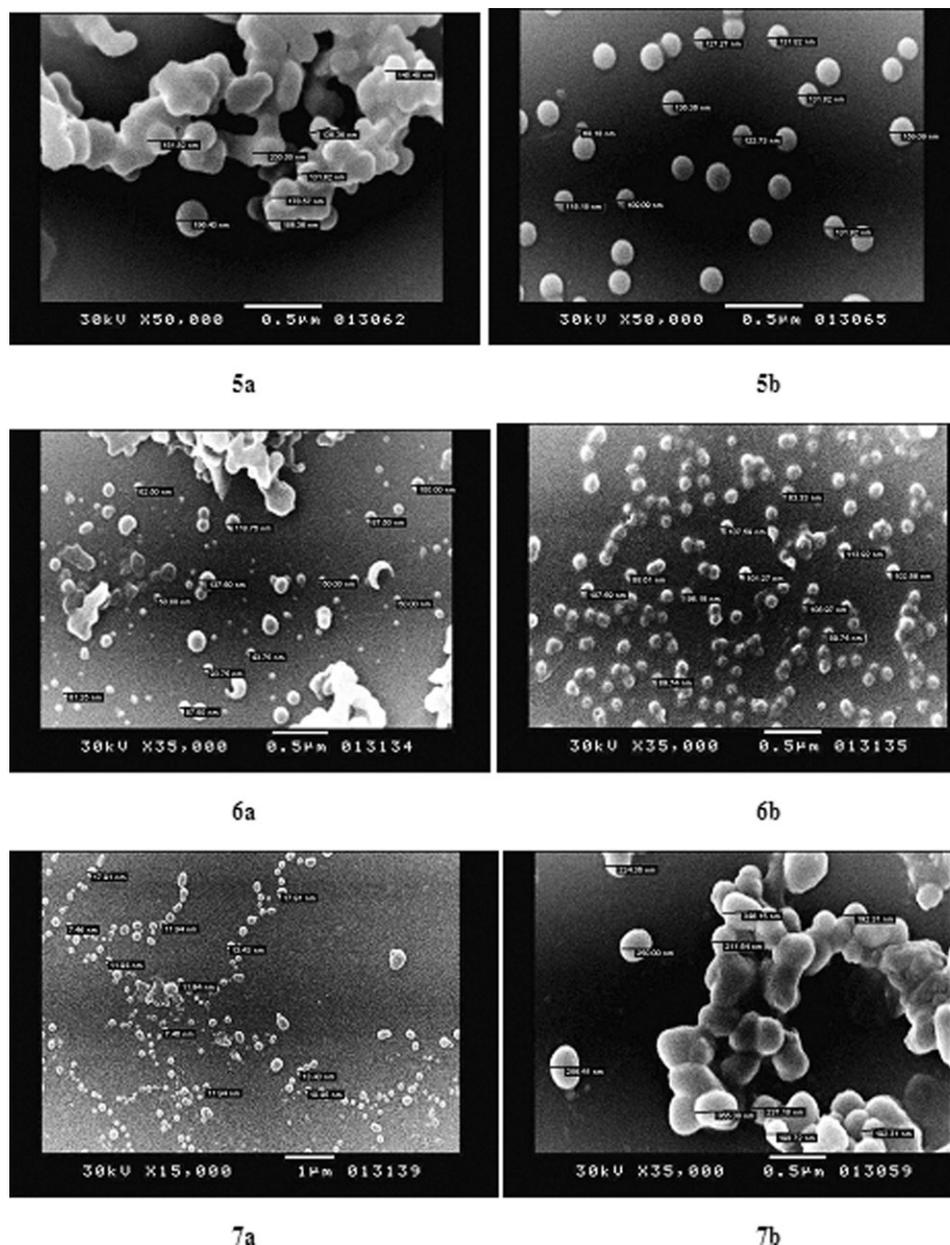
Figure 3. SEM images and particle size distributions of the sulfonated aramide nanoparticles prepared in 1,4-dioxane/water: 100 : 5 v/v (5_a, 6_a, and 7_a) and 100 : 15 v/v (5_b, 6_b, and 7_b).

nm for polymeric particles sulfonated aramide nanoparticles prepared in 1,4-dioxane/water (100/15), respectively, and the particles were obtained as well-separated spherical nanoparticle polymers with some degree of interconnection only in the case of polymer 7_b, as judged by SEM imaging. It was noteworthy that the products prepared in anhydrous reactions solutions were not obtained in particulate forms. The presence of excess water content in the reaction (e.g., 100 : 30 v/v dioxane/water) was prevented because water hydrolyzed the acid chloride to its corresponding carboxylic acid and, thus, interfered with the condensation reaction. On the basis of these results, we concluded that not only was the addition of a particular amount of water to this reaction system essential for the formation of spherical par-

ticles, but also the average diameter and the interconnection degree of these particles decreased. The tendency toward spherical particle formation of such aramides may have been correlated to the dispersion stability of the particles in the reaction solution or the precipitation mechanism of the particles.

The polymer structures were confirmed by elemental analysis and IR and UV spectroscopy. Table I compiles the physical properties of the prepared polymers. The relatively low yields obtained for the polymeric nanoparticles **5–7** could be attributed to the presence of H_3O^+ ions, which hydrolyzed the acid chloride to its corresponding carboxylic acid and, thus, inhibited the condensation reaction. However, the mixture of 1,4-dioxane with H_2O was

Table I. Yield, Elemental Analysis, Viscosity, IR, and UV Data of Polymers 5–7

Polymer no.	Yield (%)	Unit formula	Unit molecular weight	% C (Exp)	% H (Exp)	% N (Exp)	η_{inh}[a]	IR (KBr; υ, cm^{-1})	λ_{max} (nm)
5	41	$C_{32}H_{26}N_4O_6S_2$	626	61.33 (60.96)	4.18 (5.04)	8.94 (8.69)	0.92	3320, 3055, 1666, 1590, 1524, 1399, 1316, 1250, 1106.	305, 260
6	39	$C_{19}H_{15}N_3O_5S$	397	57.42 (57.01)	3.80 (3.43)	10.57 (10.46)	0.88	3323, 3055, 1688, 1590, 1525, 1447, 1316, 1247, 1105.	305 286, 260
7	39	$C_{19}H_{15}N_3O_5S \cdot H_2O$	406	56.15 (56.11)	3.94 (3.74)	10.34 (10.39)	0.80	3324, 3055, 1680, 1591, 1529, 1432, 1315, 1256, 1106.	305, 261

Exp: Experimental.
[a] η_{inh} of the polymers was measured at a concentration of 0.5 g/dL in DMSO at 30°C.

essential for many reasons, such as the control of the particle morphology and its important role in determining the polarity of the reaction solution and as a reaction accelerator.[32]

Physical Properties of the Polymers
Solubility. The pyridine-containing polymers **5–7** showed similar solubility behavior in different organic solvents. Moderate to complete dissolution (5 wt % solid content) was observed in a variety of hot aprotic solvents, such as 1-methyl-2-pyrrolidone (NMP), DMSO, and N,N-dimethylacetamide (DMAc), and in concentrated H_2SO_4, whereas **5–7** were insoluble in boiling alcoholic solvents, such as methanol, ethanol, propanol, and ethylene glycol, or in halogenated solvents, such as $CHCl_3$, CCl_4, CH_2Cl_2, and $ClCH_2CH_2Cl$, or in ethers, such as Et_2O, tetrahydrofuran, 1,4-dioxane, and 1,2-dimethoxyethane.

η_{inh}. The η_{inh} values of the polymers, a suitable criterion for the evaluation of molecular weight, were measured at a concentration of 0.5 g/dL in DMSO at 30°C and were in the range 0.80–0.92 dL/g; this indicated moderate molecular weights (Table I).

Fourier Transform Infrared Spectroscopy. The Fourier transform infrared spectra of the polyamides exhibited characteristic absorbances at 3300 and 1650 cm^{-1}, corresponding to the N—H and C=O stretching of amide groups, respectively. The bands at υ 3050 and 1600 cm^{-1} were assigned to the aromatic H—C$_{str}$ and C—C$_{str}$, respectively. Table I compiles selected IR bands of the prepared polymeric nanoparticles **5–7**.

Optical Properties. The optical properties of polymeric particles **5–7** were investigated by UV–visible spectroscopy in DMSO with a polymer concentration of about 2 mg/10 mL. Table I compiles the maximum absorbances (λ_{max}'s) of the prepared polymeric nanoparticles **5–7**. Comparison between the polyamide particles clearly revealed that the absorbance characteristics of the polymer were affected by the linear conjugated system. Particles **5–7** exhibited two identical λ_{max}'s at 305 and 260 nm, which due to $n–\pi^\star$ and $\pi–\pi^\star$ transitions, respectively. Interestingly, polymer **6**, derived from 2,6-pyridine dicarboxylic acid, exhibited an additional band at 286 nm.

Thermal Properties. The thermal properties of the polymers were evaluated by thermogravimetric (TG), DTG, and DSC techniques. Thermal data of the prepared polymers and their postulated thermal degradation analyses are compiled in Table II. Thermal results revealed that the prepared polymers had high thermal stabilities. The structure–thermal property correlation based on changes in the dicarboxylic acid monomer, as a single structural modification, demonstrated an interesting connection between a single change and the thermal properties. Polyamides **5–7** exhibited major diaminodiphenylsulfone moiety degradation processes at 460°C, with just 19.14, 45.84, and 40.19%, respectively, mass residues remaining.

The DSC measurements were achieved at a heating rate of 20°C/min in a nitrogen atmosphere. The melting temperatures (T_m's) were in the range 426–463°C. Nearly as high glass-transition temperatures (T_g's) were found for the polymers obtained because of their intractable wholly aromatic chains. The T_g's were found in the range 304–325°C, and the pyridine-containing polymer **6** showed a higher T_g degree (325°C) than the

Table II. Thermoanalytical and Kinetic Parameters of Polymers 5–7

| Polymer no.	Stage	TG peak temperature (°C)	Calculated weight loss % (Exp)	Fragment	T_m (°C)	T_g (°C)	T (°C)[a]	E_a	Arrhenius factor (A) (S^{-1})	ΔH^{*b}	ΔS^{*b}	ΔG^{*b}
5	I	24–339	39.61 (39.29)	$C_{12}H_{12}N_2O_2S$		304	133.98	24.72	2.94×10^{11}	21.3	−27.9	32.71
	II	395–993	41.37 (40.72)	$C_{13}H_9NO_3S$			465.38	203.17	5.77×10^{10}	202.0	−46.4	236.31
	R[c]		19.16 (19.14)	C_7H_5NO	463							
6	I	24–495	54.15 (53.43)	$C_7H_7NO_5S$	465	325	460	246.81	0.18×10^{10}	240.7	−75.2	295.82
	R[c]		45.84 (45.84)	$C_{12}H_{10}N_2$								
7	I	24–689	59.85 (58.80)	$C_{12}H_{11}O_4S$	426	304	460	243.25	1.04×10^{10}	237.2	−60.5	280.92
	R[c]		40.14 (40.19)	$C_7H_5N_3O_2$								

Exp: Experimental.
[a]The peak temperature from the DTG charts, [b]Values are in kJ/mol, [c]Residue.

others. This was attributed to the presence of a pyridine moiety along the polymer backbone, which restricted the free rotation of the macromolecular chains and led to an enhanced T_g.

The thermodynamic parameters of the decomposition processes of the polymers, namely, the activation energy (E_a), enthalpy (ΔH^*), entropy (ΔS^*), and Gibbs free energy change (ΔG^*) were evaluated graphically by the Coats–Redfern method.[39,40] The kinetic data obtained from the nonisothermal decomposition of the polymers are given in Table II. The pyridine-containing polyamides (**6** and **7**) demonstrated higher E_a values compared to the phenylene analogue **5**. It was noteworthy that polyamides **6** and **7** had nearly the same E_a values for the first and the second decomposition steps; this indicated a similar degradation mechanism in both compounds. According to the kinetic data obtained from the DTG curves, all of the polymers had negative ΔS^* values; this indicated ordered systems and more ordered activated states, which resulted through the chemisorption of small decomposition products.

Preparation of the Polyamide–Copper(II) Complexes. The thermal and electrical behavior of polyamides **5–7** suggested to us that we incorporate a transition metal such as copper(II) into the polymer backbone. It is often interesting to tune such properties into semiconducting polymeric nanoparticles for
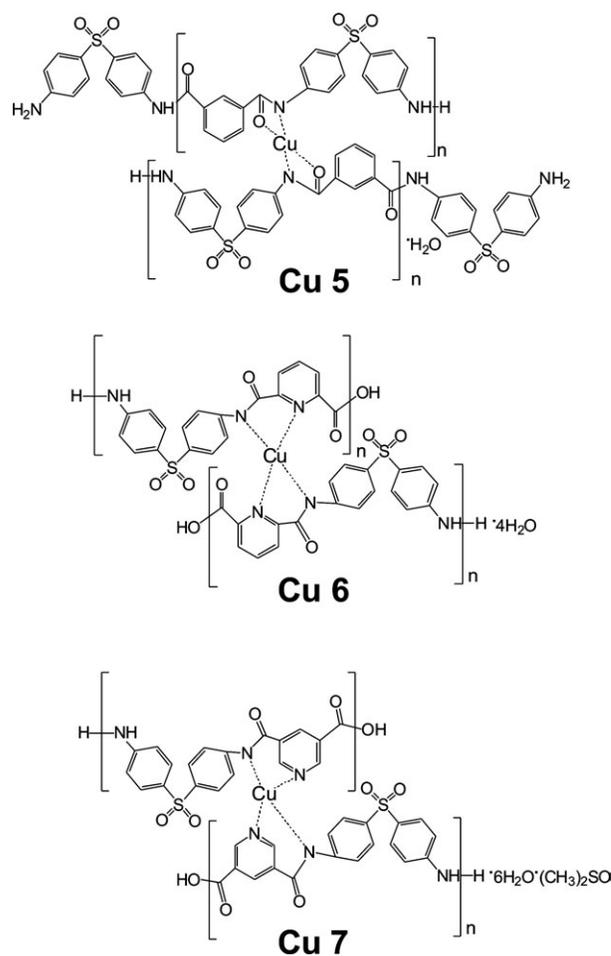
Figure 4. Proposed chemical structures of complexes **Cu5–Cu7**.

Table III. Yield, Metal Analysis, IR, UV, and ESR Data of Polymers Cu 5–Cu 7

Complex no.	Yield (%)	Unit formula	Unit MW	% C (Exp)	% H (Exp)	% N (Exp)	% Cu (Exp)	IR (KBr; v cm^{-1})	λ_{max}	$g_\perp$	$g_\parallel$
Cu 5	88	$(C_{32}H_{25}N_4O_6S_2)_2$ Cu$_{1/2}$	1281.5	59.92 (59.09)	3.90 (4.18)	8.74 (6.72)	2.47 (2.70)	3321, 3103, 1671, 1591, 1526, 1397, 835,721, 576	325, 260, 475	1.89	2.04
Cu 6	91	$(C_{19}H_{14}N_3O_5S)_2$ Cu·4H$_2$O	927.5	49.16 (48.99)	3.88 (4.70)	9.05 (9.17)	7.42 (7.44)	3355, 1671, 1592, 1527, 1381. 832, 721, 691, 578, 554	365, 400, 670	1.92	2.09
Cu 7	91	$(C_{19}H_{14}N_3O_5S)_2$ Cu·6H$_2$O·(CH$_3$)$_2$SO	1000.5	48.60 (48.17)	4.05 (3.23)	8.39 (8.65)	7.42 (7.71)	3323, 3104, 1682, 1592, 1530, 1400, 837, 720, 690, 579	350, 261, 406	1.93	2.10

many industrial applications. The complexation reaction was carried out by careful addition of Cu(OAc)$_2$·H$_2$O (1.2 equiv) to the stirred hot solution of the polymer in DMSO at 80–90°C for 4 h. The Cu(II) ions complexed with a polymer repeating unit at a ratio of 1 : 2 and the complexes structures **Cu5–Cu7** (Figure 4) are proposed on the basis of IR, UV, ESR, and elemental analyses (Table III). The elemental analysis data (Table III) showed that the metal-to-polymer ratio was 1 : 2, and this was in good agreement with the calculated values. The pyridine-containing polymers **Cu6** and **Cu7** showed similar sites of metal coordination. The metal ions could be accommodated inside the inner cavity made by the pyridine nitrogen atom with two hydrogen amide atoms pointing toward the cavity, whereas the carbonyl groups were directed outside of the inner cavity to produce five- and six-membered chelate rings, respectively. The appearance of the sharp Cu—N bands at v 690 cm^{-1} in these complexes unambiguously proved that the pyridine nitrogen atom represented the central binding site.[41] The copper complexes **Cu5–Cu7** showed bands around v 1660 and 3300 cm^{-1}, which corresponded to the amide C=O and NH, respectively.

The complexes exhibited λ_{max}'s at 324 and 260 nm (Cu 5), 365 and 260 nm (**Cu6**), and 350 and 261 nm (**Cu7**) due to n-$\pi^\star$ and π–$\pi^\star$ transitions. The bands at 475, 400, and 406 nm were attributed to the ligand–metal charge-transfer transitions from the conjugated n and p orbitals of the donor to d orbitals of the metal. In addition, **Cu6** exhibited a highly redshifted band at λ_{max} 670 nm due to $^2B_{1g}{\rightarrow}^2B_{2g}$ transition; this indicated a square planar geometry in the metal complex.[42]

The ESR parameters of the copper(II) complexes **Cu5–Cu7** are presented in Table III. The ESR spectra of the copper compounds in the polycrystalline state at room temperature were quite similar and exhibited typical axial spectra with spectroscopic splitting factor parallel to the principle axis $g_\parallel$ > spectroscopic splitting factor perpendicular to the principle axis $g_\perp$ features; this indicated a rbital ground state wave function d_{x2-y2} ground state and was consistent with a square planar stereochemistry around a copper(II) center.[43] The spectra had hyperfine splitting parallel to the principle axis $A_\parallel$ > 100 × 10^{-4} cm^{-1}; this prevented a pseudo tetrahedral structure and, thus, supported a square planar geometry around a Cu(II) center. In an axial symmetry, spectroscopic splitting factor g values are related by the expression: value for the free electron $G = (g_\parallel - 2)/(g_\perp - 2)$, which measures the exchange interactions between copper centers and polycrystalline solids. The calculated G values were less than 4, which suggested considerable exchange interaction in solid complexes.[44]

Thermal analysis of the copper complexes **Cu5–Cu7** revealed a high thermal stability up to 500°C. Figure 7 (shown later) shows the TG/DTG curves of these complexes, whereas their thermoanalytical and kinetic parameters are compiled in Table IV. Interestingly, the thermal analysis data of this series demonstrated similar major amide linkage degradation at 450°C. The total mass loss values of polymers **Cu5** and **Cu7** showed that 82% of the mass loss corresponded to the removal of the adsorbed water, degradation of the end group, and the diaminodiphenylsulfone moiety, respectively, and left 16% attributable

Table IV. Thermoanalytical and Kinetic Parameters of Polymers Cu 5–Cu 7

Complex no.	Stage	TG peak temperature (°C)	Calculated weight loss % (Exp)	Fragment	T^a	E_a	Arrhenius factor (A) (S^{-1})	ΔH^{*b}	ΔS^{*b}	ΔG^{*b}
Cu5	I	24-200	38.39 (38.15)	$(C_{12}H_{10}N_2O_2S)_2$	130	39.36	1.14×10^{10}	36.26	−54.25	56.49
	II	220-700	42.76 (43.15)	$(C_{13}H_{10}N_2O_3S)_2$	450	197.6	3.4×10^{11}	191.58	−31.44	214.31
	R^c		19.93 (18.70)	$CuO + 4 \times CO_2$						
Cu6	I	24-200	7.74 (7.47)	$4H_2O$	130	38.35	1.23×10^{11}	35.66	−33.25	46.40
	II	220-700	59.08 (59.49)	$[C_{13}H_{10}N_2O_3S]_2$	450	66.87	2.69×10^{11}	60.85	−52.57	98.86
	R^c		32.93 (33.04)	$[C_6H_3NO_2]_2 + CuO$						
Cu7	I	24-200	10.79 (10.04)	$6H_2O$	125	98.78	2.17×10^{10}	95.47	−49.43	115.14
	II	220-700	72.46 (71.98)	$C_{36}H_{24}N_6O_3S_2+$	400	71.73	0.4×10^{10}	66.13	−63.56	111.59
	R^c		16.74 (16.09)	$(CH_3)_2SO$ $CuO + 2CO_2$						

Exp: Experimental.
[a]The peak temperature from the DTG charts, [b]Values are in kJ/mol, [c]Residue.

to CuO and CO_2 residues.[45] DSC curves illustrated neither melting endotherm peaks (T_m's) nor T_g's for the investigated complexes **Cu5–Cu7** and, thus, revealed the amorphous nature of these polymers.

The kinetic data obtained from the nonisothermal decomposition of the complexes are given in Table IV. The results reveal that the last decomposition step in the case of the pyridine-containing polymers **Cu6** and **Cu7** had nearly the same E_a values. Additionally, the last decomposition step in the phenylene analogue **Cu5** exhibited a high E_a value, which may have been due to the thermal stability of the remaining residue at this stage. According to the kinetic data obtained from DTG curves, all polymers had a negative ΔS^*, which indicated ordered systems and more ordered activation states, which may have been a result of the chemisorption of other small decomposition products.

Electrical Properties

Conjugated polymers have been studied for many years[46] because of their attractive electronic and optoelectronic properties. One of the most important goals in the field of materials science is to develop narrow-band-gap polymers. Indeed, a narrow band gap can be obtained by starting from a monomer that already has a narrow highest occupied molecular orbital–lowest unoccupied molecular orbital energy[47] separation. Hence, the search for a low-energy-gap parent molecules is a key step in designing conductive polymers. On the basis of this hypothesis, many studies on organic conjugated systems combined with donor–acceptor groups or fused with other conjugated rings to reduce their band gaps have been reported.[48] Such data have attracted interest in many areas of materials research, including in organic light-emitting displays, field-effect transistors, solar cells, and switching devices.

The direct-current (dc) electrical conductivity of polymers **5–7** revealed different behavior. The relations between the real and imaginary parts of the impedance at different temperatures were plotted for these samples. The behavior of the Cole–Cole diagrams was characterized by semicircles originating from the origin with no overlap at all temperatures; this indicated that the

samples obeyed the relaxation of Debye model and also indicated the unavailability of the electrode effect during measurement.[49] Extrapolation of the high-frequency limit of the semicircle intercepts with the real axis gave the value of the bulk resistance for the samples, from which the dc conductivity was calculated. The temperature dependence versus dc conductivity for polymers **5–7**, plotted as direct current electrical conductivity σ_{dc} (Ω^{-1} cm^{-1}) versus peak temperature T (K), is presented in Figure 5. Interestingly, the dc conductivity of the pyridine-containing polymers **6** and **7** increased with increasing temperature, as determined from the plot of electrical conductivity σ (Ω^{-1} cm^{-1}) versus T (K). This behavior indicated the semiconducting nature of these samples, as it obeyed the three-dimensional Mott variable-range hopping model,[50] which describes the temperature dependence of the conductivity of disordered semiconducting materials. However, in case of the phenylene-containing polymer **5**, the conductivity strongly decreased with temperatures in the range 290–300 K.

Metal chelation with copper produced polymeric complexes that had better optical and electrical properties than the ligands. Again, the behavior of the Cole–Cole diagrams was characterized by semicircles originating from the origin with no overlap
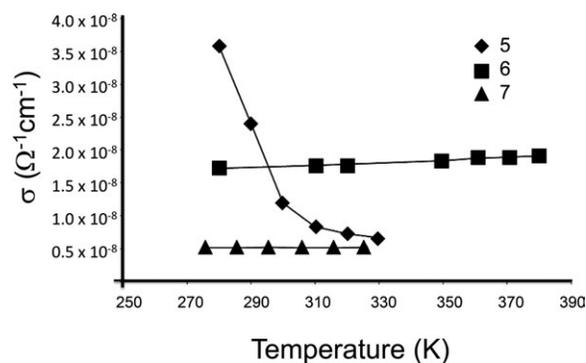
Figure 5. Temperature dependence of the dc electrical conductivity for polymers 5–7.
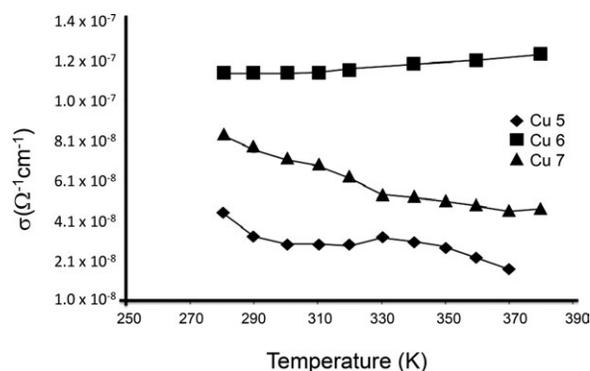
Figure 6. Temperature dependence of the electrical conductivity for polymers Cu 5–Cu 7.

at all temperatures; this indicated that the samples obeyed the relaxation of Debye model and also indicated the unavailability of an electrode effect during measurement. The temperature dependence versus dc conductivity for the copper complexes **Cu5–Cu7**, plotted as σ (Ω^{-1} cm^{-1}) versus T (K), is presented in Figure 6, and the σ (Ω^{-1} cm^{-1}) values of the prepared polymers at 310 K are given in Table V. The conductivity of the complex **Cu6** was seven times higher than that of its ligand (**6**), and the complex exhibited a semiconducting character as the conductivity increased with increasing temperature. In contrast, the conductivity of **Cu7** exhibited a metallic character, and its value was 13 times higher than that of its ligand (**7**). In the case of **Cu5**, the conductivity revealed a fourfold improvement compared to that of **5** and also exhibited a metallic character. It was obvious that polymer structural variations played a major role in determining the electrical conduction efficiency of the complexes, and the recorded conductivity values were in the order **Cu6 > Cu7 > Cu5**.

Dielectric Loss Analysis
Dielectric analysis is an informative technique used to determine the molecular motions and structural relaxations present in polymeric materials possessing permanent dipole moments.[51] In dielectric measurements, the material is exposed to an alternating electric field, which is generated by the application of a sinusoidal voltage; the process causes alignment of dipoles in the material, which results in polarization. The polarization will cause the output current to lag behind the applied electric field by a phase shift angle. The magnitude of the phase shift angle is determined by the measurement of the resulting current. The capacitance and conductance are then calculated from the relationship between the applied voltage, measured current, and phase shift angle.[52] The capacitance and conductance of the material are measured over a range of temperatures and frequencies and are related to the dielectric permittivity (ε') and the dielectric loss factor (ε''), respectively. ε' represents the amount of dipole alignment and ε'' measures the energy required to align dipoles or move ions. The loss in dielectrics, known as the loss tangent (tan δ), ε', and ε'' are defined as given in the following equation:

$$\tan \delta(\omega) = \varepsilon''(\omega)/\varepsilon'(\omega)$$

According to this definition, tan $\delta(\omega)$ describes the ratio between the dissipated and the reversibly exchanged work (i.e.,

an energy that during one half-period is stored in the driven system and during the successive half-period is completely returned).[53] Figure 7 (shown later) shows the variation of tan δ with frequency of polymers **5–7** and their complexes **Cu5–Cu7** at 280 K in the frequency range 0.1 to 5 $\times$ 10^3 kHz. In all of the prepared samples, there were various bond functions that could act as a matrix and provide electrical dipoles. Dielectric losses from ligands **5–7** mainly stemmed from contributions of these functional groups, whereas those losses from the hybrids **Cu5–Cu7** stemmed from the contribution of both metal and organic functional groups. The loss spectra were characterized by peaks appearing at characteristic frequencies for the investigated samples; this suggested the presence of relaxing dipoles in all of them. The strength and frequency of relaxation depend on the characteristic property of dipolar relaxation. Metal chelation with copper ions with these polymers had a significant effect on the loss spectra. Moreover, the peak positions did not change with increasing temperature in the range 280–380 K; this indicated a nonthermally activated process. This behavior suggests that a given field, in the steady state, produced a constant polarization, regardless of the temperature.[54] This could be understood in terms of the polarization being limited by nonthermal forces, that is, by elastic constraint, instead of being limited by thermal agitation, as in the classical Debye process.

The results show that the tan δ values of complexes **Cu5** and **Cu7** in the frequency range 3000–4000 KHz increased, and the peaks shifted toward the lower frequency upon doping. In the case of **Cu7**, a new loss peak was found at frequency of about 2700 KHz on doping. The appearance of this peak was attributed to the relaxation phenomena of the polymer.[55] The tangent loss peaks for polymers **Cu5** and **Cu7** shifted toward higher frequency on metal chelation. This suggested that there was an increase in the amorphous content in the complexes relative to their parent ligands **5** and **7**, respectively. The metal ion sped up the segmental motion by increasing the available free volume. This was evidenced by the peak shifting to higher frequency, which thereby reduced the relaxation time. The relatively fast segmental motion coupled with mobile ions enhanced the transport properties on chelation. However, a decrease in the tan δ values of **Cu5** and **Cu7** was observed in the lower frequency region. Because tan $\delta = \varepsilon''/\varepsilon'$, on metal chelation, the ratio of energy loss was increased compared to the energy storage in the dielectric. The higher value of ε'' at low frequency was due to the free charge motion within the materials. The ε'' increases in the lower frequency region reflected the enhancement of mobility of the charge carrier upon complexation.

Interestingly, for **Cu5**, Figure 7(a) exhibited four well-resolved and symmetric peaks. It is noteworthy that the shoulder

Table V. Electrical Conductivity of Polymers **5–7** and their Complexes Cu 5–Cu 7 at 310 K

Polymer no.	σ (Ω^{-1} cm^{-1})	Complex no.	σ (Ω^{-1} cm^{-1})
5	8.43×10^{-9}	**Cu5**	2.95×10^{-8}
6	1.77×10^{-8}	**Cu6**	1.15×10^{-7}
7	5.22×10^{-9}	**Cu7**	6.85×10^{-8}
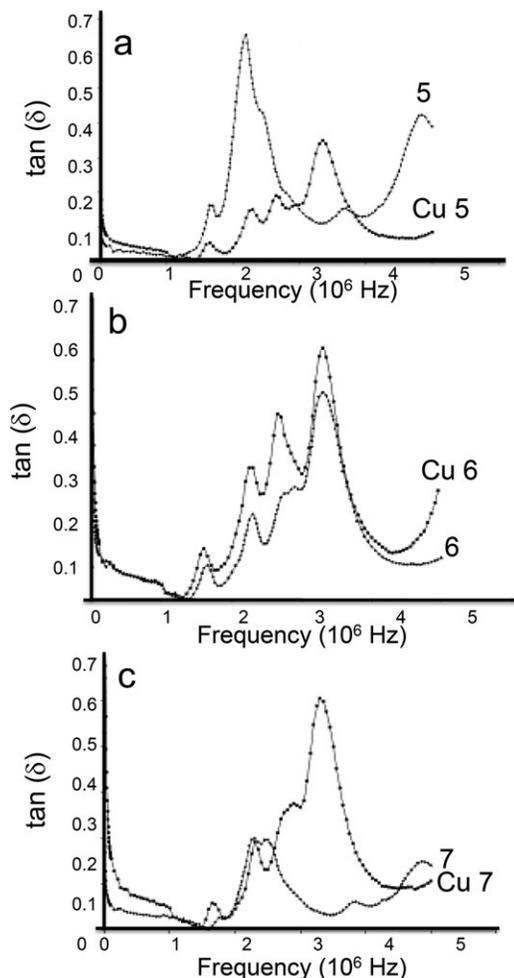
Figure 7. Tan δ versus frequency for polymers: (a) **5** (**Cu5**), (b) **6** (**Cu6**), and (c) **7** (**Cu7**).

observed in the loss spectra of **5** changed to two well-resolved peaks in the complex **Cu5** with a considerable reduction in the tan δ value. Similar loss behaviors in compounds **6**, **7**, **Cu6**, and **Cu7** were observed [Figure 7(b,c), respectively]. It is also note-
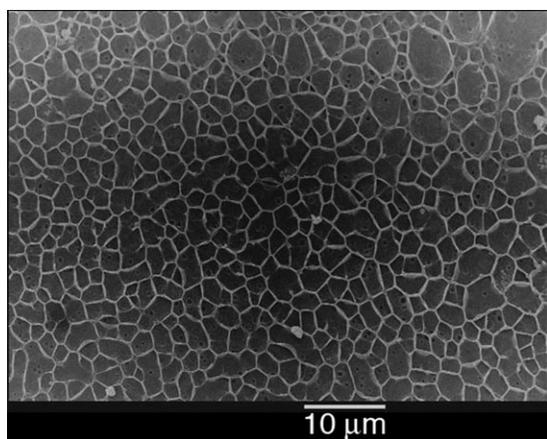
Figure 8. SEM images of the thin film of polymer formed by the mixture of polymer **5** with H_2O.
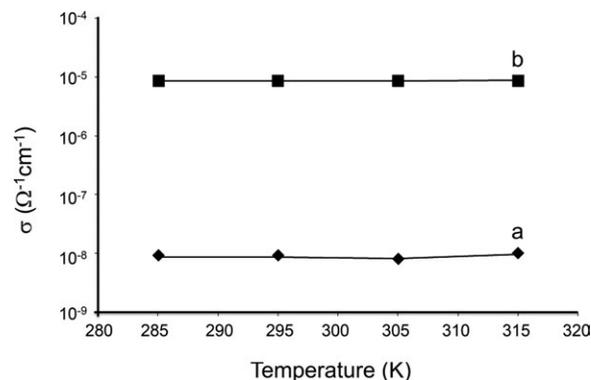

Figure 9. σ_{dc} (Ω^{-1} cm^{-1}) versus T (K) of the polymer **5** film: (a) transverse and (b) longitudinal conductivities.

worthy that all loss peaks for these samples, shown on a linear frequency scale, appeared in the range of 1 decade and did not overlap. The reported dielectric results reveal anomalous behavior, which, to the best of our knowledge, has not been reported by earlier researchers for similar polymers. The common behavior of the loss peaks in a polymer is that each peak covers more than 1 decade, and hence, tan δ is always plotted against the logarithm of frequency,[56,57] whereas in case of single crystal samples, the loss factor spectrum contains sharp loss peaks in the range 100–300 kHz.[54] In our data, the recorded loss peaks retained their shape and their amplitude with increasing temperature. The implication of this behavior was that in the steady state, a given field produced a constant polarization, regardless of the temperature. This could be understood in terms of the polarization being limited by nonthermal forces, that is, by elastic constraints, instead of being limited by thermal agitation, as in the classical Debye process.

Formation of the Thin Film of Polymer 5

The addition of water to the polymer solution **5** applied on a flat glass surface produced a white flexible thin film of the polymer with a thickness equal to 250 μm (micrometer measurement). As judged by the SEM image (Figure 8), the film had a microporous layer structure. In addition, the formed film had the following properties: (1) it exhibited a thermal shrinking at 60–70°C; (2) the thin film was porous, and the material was
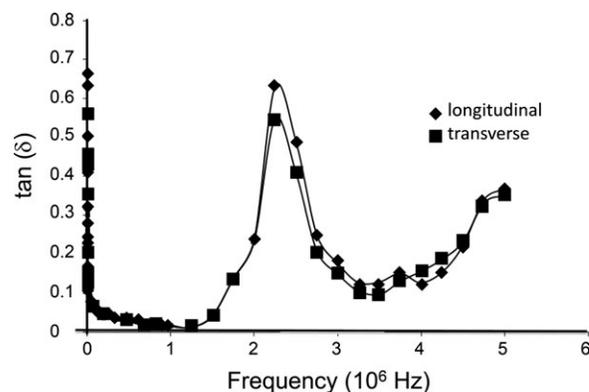
Figure 10. Tan δ versus frequency for the transverse and longitudinal directions for the thin film of **5** at 285 K.

insoluble in water, methanol, ethanol, and acetic and formic acids; and (3) in conducting transverse dc conductivity (Figure 9), the film exhibited a low semiconducting nature ($\sigma = 10^{-9}$ Ω^{-1} cm^{-1}), whereas in case of longitudinal dc conductivity, the film exhibited a better semiconducting nature ($\sigma = 10^{-6}$ Ω^{-1} cm^{-1}).

Figure 10 shows the variation of tan δ with frequency for the transverse and longitudinal directions of the polymer film **5** at 285 K in the frequency range $0.1 \times 10^3 - 5.0 \times 10^3$ kHz. The loss spectra were characterized by similar peaks appearing at the same frequencies; this suggested the presence of relaxing dipoles in both directions.

CONCLUSIONS

The ultrasonication of acid chlorides of isophthallic and 2,6-pyridine- and 3,5-pyridine-dicarboxylic acids with **4** in 15% dioxane/water followed by centrifugal separation provided respective well-separated spherical aramides nanoparticles with a 100–230-nm average diameter, as judged by SEM images. The reactions of copper(II) ions with these particles furnished copper–polymer complexes in a 1 : 2 ratio, and the reported structures were based on their IR, UV, ESR, and elemental analysis data. The thermal properties were evaluated by TG/DTG and DSC techniques, and the thermodynamic parameters of the decomposition processes were evaluated graphically with the Coats–Redfern method. The electrical conductivity results show that the electrical conductivity of the pyridine-containing polymers increased with increasing temperature, and this behavior was indicative of a semiconducting nature. Metal chelation with copper produced polymeric complexes that had better optical and electrical properties than the ligands. Dielectric loss analysis studies showed spectral peaks appearing at characteristic frequencies; this suggested the presence of relaxing dipoles in all of the polymers. All of the loss peaks were shown on a linear frequency scale and appeared in the range of 1 decade, and no overlapping was observed in any of the samples, whereas in a normal polymer's dielectric loss behavior, each peak covers more than 1 decade, and hence, tan δ is always plotted against the logarithm of frequency. Moreover, the peak positions did not change with increasing temperature; this indicated a non-thermally activated process. It was noteworthy that the reported dielectric results revealed anomalous behavior, which has not been reported earlier in such polymeric analogues; the polarization in these cases was limited by nonthermal forces, and a steady-state constant polarization was produced by a field. A simple method for the formation of a microporous semiconducting thin film of polymer derived from isophthalic acid and 4,4′-diaminodiphenylsulfone was also described.

REFERENCES

1. Cassidy, P. E. Thermally Stable Polymers; Marcel Dekker: New York, **1980.**

2. Yang, H. H. Aromatic High-Strength Fibers; Wiley: New York, **1989.**

3. Fink, J. K. High Performance Polymers; William Andrew: New York, **2008.**

4. Vollbracht, L. In Aromatic Polyamides: Comprehensive Polymer Science; Allen, G., Bevington, B., Eastmond, G. V., Ledwith, A., Russo, S., Sigwald, P., Eds.; Pergamon: Oxford, **1989;** Vol. 5, p 373.

5. Choi, K. H.; Jung, J. C. *Macromol. Mater. Eng.* **2004,** *289*, 737.

6. Hearle, J. W. S. High Performance Fibers; Woodhead: Cambridge, United Kingdom, **2001.**

7. Nelson, G. L.; Wilkie, C. A. Fire and Polymers; American Chemical Society: Washington, DC, **2003.**

8. Odian, G. Principles of Polymerization, 4th ed.; Wiley: Hoboken, NJ, **2004.**

9. Spiliopoulos, I. K.; Mikroyannidis, J. A. *Macromolecules* **1998,** *31*, 1236.

10. Eastmond, G. C.; Paprotny, J.; Irwin, R. S. *Polymer.* **1999,** *40*, 469.

11. Liou, G. S.; Hsiao, S. H.; Ishida, M.; Kakimoto, M.; Imai, Y. *J. Polym. Sci. Part A: Polym. Chem.* **2002,** *40*, 2810.

12. Hsiao, S. H.; Chen, W. T. J. *Polym. Sci. Part A: Polym. Chem.* **2003,** *41*, 420.

13. Yang, C. P.; Hsiao, S. H.; Chung, C. L. *Polym. Int.* **2005,** *54*, 716.

14. Hsiao, S. J.; Yang, C. P.; Huang, S. C. *J. Polym. Sci. Part A: Polym. Chem.* **2004,** *42*, 2377.

15. Wang, X. L.; Li, Y. F.; Gong, C. L.; Ma, T.; Yang, F. C. *J. Fluorine. Chem.* **2008,** *129*, 56.

16. Manami, H.; Nakazawa, M.; Oishi, Y.; Kakimoto, M.; Imai, Y. *J. Polym. Sci. Part A: Polym. Chem.* **1990,** *28*, 465.

17. Idage, S. B.; Idage, B. B.; Shinde, B. M.; Vernekar, S. P. *J. Polym. Sci. Part A: Polym. Chem.* **1989,** *27*, 583.

18. Brode, G. L.; Kawakami, J. H.; Kwiatkowski, G. T.; Bedwin, A. W. *J. Polym. Sci. Part A: Polym. Chem.* **1974,** *12*, 575.

19. Carlier, V.; Devaux, J.; Legras, R.; McGrail, P. T. *Macromolecules* **1992,** *25*, 6646.

20. (a) Guo, P.; Chen, P.; Liu, M. *Nanoscale. Res. Lett.* **2011,** *6*, 529; (b) Hurst, S. J.; Payne, E. K.; Qin, L.; Mirkin, C. A. *Angew. Chem. Int. Ed.* **2006,** *45*, 2672; (c) Tian, B.; Kempa, T. J.; Lieber, C. M. *Chem. Soc. Rev.* **2009,** *38*, 16; (d) Heath, J. R. *Acc. Chem. Res.* **2008,** *41*, 1609; (e) Jiea, J.; Zhang, W.; Bello, I.; Lee, C.-S.; Lee, S.-T. *Nano. Today.* **2010,** *5*, 313; (f) Shimizu, T.; Masuda, M.; Minamikawa, H. *Chem. Rev.* **2005,** *105*, 1401; (g) Zang, L.; Che, Y.; Moore, J. S. *Acc. Chem. Res.* **2008,** *41*, 1596; (h) Yamamoto, T.; Fukushima, T.; Aida, T. *Adv. Polym. Sci.* **2008,** *220*, 1; (i) Zhao, Y. S.; Fu, H.; Peng, A.; Ma, Y.; Liao, Q.; Yao, J. *Acc. Chem. Res.* **2010,** *43*, 409.

21. (a) Mulvihill, M. J.; Ling, X. Y.; Henzie, J.; Yang, P. *J. Am. Chem. Soc.* **2010,** *132*, 268; (b) Liu, X.-M.; Fu, S.-Y.; Xiao, H.-M.; Huang, C.-J. *J. Solid. State. Chem.* **2005,** *178*, 2798; (c) Raula, M.; Rashid, M. H.; Paira, T. K.; Dinda, E.; Mandal, T. K. *Langmuir.* **2010,** *26*, 8769; (d) Wang, H.; Shao,

W.; Gu, F.; Zhang, L.; Lu, M.; Li, C. *Inorg. Chem.* **2009,** *48,* 9732.

22. Ni, H.; Kawaguchi, H. *J. Polym. Sci. Part A: Polym. Chem.* **2004,** *42,* 2833.

23. Lin, C.; Zang, Z.; Zheng, J.; Liu, M.; Zhu, X. X. *Macromol. Rapid. Commun.* **2004,** *25,* 1719.

24. Vennes, M.; Zentel, R. *Macromol. Chem. Phys.* **2004,** *205,* 2303.

25. Imbert-Laurenceau, E.; Berger, M. C.; Pavon-Djavid, G.; Jouan, A.; Migonney, V. *Polymer.* **2005,** *46,* 1277.

26. Li, J.; Zhang, J. Z. *Coord. Chem. Rev.* **2009,** *253,* 3015.

27. Gu, Z.; Chen, X. Y.; Shen, Q. S.; Ge, H. X.; Xu, H. H. *Polymer.* **2010,** *51,* 902.

28. (a) Yuan, J.; Müller, A. H. E. *Polymer.* **2010,** *51,* 4015; (b) Lu, X.; Zhang, W.; Wang, C.; Wen, T. C.; Wei, Y. *Prog. Polym. Sci.* **2011,** *36,* 671; (c) Barth, S.; Hernandez-Ramirez, F.; Holmes, J. D.; Romano-Rodriguez, A. *Prog. Mater. Sci.* **2010,** *55,* 563.

29. Hassan, H. H. A. M.; Elhusseiny, A. F.; Sweyllam, A. M. *J. Macromol. Sci. Part A: Polym. Chem.* **2010,** *47,* 521.

30. Hassan, H. H. A. M.; Elhusseiny, A. F.; Sweyllam, A. M. *J. Macromol. Sci. Part A: Polym. Chem.* **2011,** *48,* 73.

31. Hassan, H. H. A. M.; Elhusseiny, A. F.; Sweyllam, A. M. *J. Mol. Struct.* **2011,** *1001,* 89.

32. Yoshioka, Y.; Asao, K.; Yamamoto, K.; Tachi, H. *Macromol. React. Eng.* **2007,** *1,* 222.

33. Mamo, A.; Aureliano, A.; Battiato, S.; Cicala, G.; Samperi, F.; Scamporrino, A.; Recca, A. *Polymer.* **2010,** *51,* 2972.

34. Balzani, V. Electron Transfer in Chemistry; Wiley: Weinheim, **2001.**

35. Ge, Z.; Yang, S.; Tao, Z.; Liu, J.; Fan, L. *Polymer.* **2004,** *45,* 3627.

36. Tamami, B.; Yeganeh, H. *Eur. Polym. J.* **2002,** *3,* 933.

37. Schwarzenbach, G. Complexometric Titration; Irving, H., Ed.; Methnen: London, **1957.**

38. Sharma, K. R. Nanostructuring Operations in Nanoscale Science and Engineering; McGraw-Hill: New York, **2010.**

39. Coats, A. W.; Redfern, J. P. *Nature.* **1961,** *201,* 68.

40. Johnson, D. W.; Gallagher, P. K. *J. Phys. Chem.* **1972,** *76,* 1474.

41. Singh, B. K.; Jetley, U. K.; Sharma, R. K.; Garg, B. S. *Spectrochim. Acta. Part A.* **2007,** *68,* 63.

42. Chessman, T. P.; Holl, D.; Waters, T. N. *J. Chem. Soc. A.* **1966,** 694.

43. Hathaway, B. J.; Billing, D. E. *Coord. Chem. Rev.* **1970,** *5,* 143.

44. Ruf, M.; Noll, B.; Groner, M.; Yee, G. T.; Pierpont, C. G. *Inorg. Chem.* **1997,** *36,* 4860.

45. (a) Panchani, S. C.; Kharadi, G. J.; Patel, K. D. *Polym. Mat.* **2010,** *59,* 60; (b) Kharadi, G. J.; Patel, K. D. *Appl. Organomet. Chem.* **2010,** *24,* 332.

46. Skotheim, T. A.; Elsenbaumer, R. L.; Reynolds, J. R. Handbook of Conducting Polymers; Marcel Dekker: New York, **1998.**

47. Tanaka, S.; Yamashita, Y. *Synth. Met.* **1997,** *84,* 229.

48. Mott, N. F.; Davis, E. Electronic Processes in Non-Crystalline Materials; Clarendon: Oxford, **1979.**

49. Dutta, P.; Biswas, S.; Ghosh, M.; De, S. K.; Chatterjee, S. *Synth. Met.* **2000,** *122,* 455.

50. McCrun, N. G.; Read, B. E.; Williams, G. Annelastic and Dielectric Effects in Polymeric Solids; Dover: New York, **1967.**

51. Avakian, P.; Starkweather, H. W., Jr.; Kampert, W. G. In Handbook of Thermal Analysis and Calorimetry; Cheng, E. Z. D., Ed.; Elsevier: New York, **2002;** Vol. *3,* p 147.

52. Strobl, G. The Physics of Polymers: Concepts for Understanding Their Structures and Behavior; Springer: Berlin, **2007.**

53. Dillip, K. P.; Choudhary, R. N. P.; Samantary, B. K. *Int. J. Electrochem. Sci.* **2008,** *3,* 597.

54. Jonsher, A. K. Dielectric Relaxation in Solids; Chelsa Dielectrics: London, **1983.**

55. Broad Band Dielectric Spectroscopy; Kremer, F., Schonhals, A., Eds.; Springer-Verlag: Berlin, **2003.**

56. Tareev, B. Physics of Dielectric Materials; Mir: Moscow, **1979.**

57. Shankar, M. V.; Varma, K. B. R. *Bull. Mater. Sci.* **1996,** *19,* 791.